The following publication H. Li and W. Lin, "An Ultracompact Shared-Radiator Electrically Small Huygens Dual-Circularly Polarized Antenna," in IEEE Transactions on Antennas and Propagation, vol. 73, no. 7, pp. 4915-4920, July 2025 is available at https://doi.org/10.1109/TAP.2025.3550449.

An Ultracompact Shared-Radiator Electrically Small Huygens Dual-Circularly-Polarized Antenna

Huacheng Li, Graduate Student Member, IEEE, and Wei Lin, Senior Member, IEEE

Abstract-A novel electrically small shared-radiator Huygens dualcircularly-polarized (HDCP) antenna is developed that features an ultracompact size, i.e., π (0.12 λ_c)² × 0.06 λ_c = 0.0027 λ_c ³ (ka = 0.78) at 915 MHz. A shared-radiator is formed by a pair of orthogonally placed Huygens linearly-polarized (HLP) antennas. HDCP beams, i.e., left-hand (LHCP) and right-hand CP (RHCP) Huygens beams, can be simultaneously excited by an '8'-shaped feed-line as the driven element. To compensate for the inductive impedance, an innovative and compact LC matching network is developed to match both ports to standard 50 Ω transmission lines. The measured results of the prototype agree reasonably with the simulated ones. The results showcase a good isolation lower than -16 dB between the two input ports and a wide measured (simulated) 3-dB AR beamwidth of 120° (144°). Additionally, the measured peak realized gain values for LHCP and RHCP beams are consistent, e.g., 2.8 dBic and 2.6 dBic, respectively. As an ultracompact DCP antenna, it is an ideal candidate for wireless applications that require DCP performance along with compact system size, e.g., batteryfree IoT ecosystem with simultaneous wireless power and data transmission.

Index Terms—Electrically small antennas, dual circular polarization, Huygens dipole antenna, shared radiator.

I. Introduction

ELECTRICALLY small Antennas (ESAs) with circular polarization (CP) have received increasing attention in recent years for the rapid development of modern wireless technologies such as RFID, wireless power transfer (WPT), and Internet of Things (IoT) systems and their requirement for miniaturized antennas [1], [2], [3]. Compared with the linearly polarized (LP) antenna, the CP property is desired because it can effectively overcome polarization mismatch problems and multipath distortions [4]. Many efforts have been made to design miniaturized CP antennas as in [5], and [6]. Nevertheless, these antennas can only exabit a single polarization mode (left-hand circular polarization, i.e., LHCP, or right-hand circular polarization i.e., RHCP). On the other hand, due to the growing demands for compact and multifunctional wireless systems, polarization diversity technology is gaining popularity recently in both academia and industry. Since it supports both polarization states, a single antenna or array with dual-CP (DCP) radiation is much preferred. It not only enhances the channel capacity but also reduces the complexity and cost of the entire wireless system [7], [8].

Extensive research has been reported to design DCP antennas for various wireless applications as in [9] - [25]. In general, three common design methodologies have been utilized. The most popular method involves exciting LP radiators using parallel or series feeding networks, e.g., a combination of LP radiators with 90-degree hybrid couplers [9]-[12], two-port aperture-coupled [13]-[15] or

Manuscript received xx, 2024; This work was supported by

Huacheng Li and Wei Lin are with the Department of Electrical and Electronic Engineering, The Hong Kong Polytechnic University, Hong Kong SAR, China (e-mail: w.lin@polyu.edu.hk).

Color versions of one or more of the figures in this communication are available online at http://ieeexplore.ieee.org.

proximate-coupled [16], [17] feeding network, etc. Another design strategy is the direct excitation of CP radiators using a novel feeding scheme [18]-[21], or the combination of two radiators with different CP radiations [22], [23]. The third approach utilizes a CP polarizer to transform the dual-LP radiation to DCP waves [24], [25]. However, it should be emphasized that all the DCP antennas mentioned above are electrically large. They are not suitable for wireless applications that require a compact footprint like the IoT system. To the best of our knowledge, designing a compact antenna with DCP characteristics is very challenging due to the difficulty of maintaining high port isolation in a restricted size. Moreover, it is even more challenging if the DCP antenna can achieve wide beamwidth, i.e., overlapped 3-dB realized gain and AR beamwidth.

In recent years, electrically small Huygens dipole antennas (HDAs) invented by Ziolkowski [26] have attracted much attention owing to their advantages such as electrical small size, high directivities, large front-to-back ratio, and wide beamwidths. The versatility of HDAs in terms of shape and feeding mechanisms offers antenna designers significant flexibility to choose from various configurations to achieve specific radiation characteristics, including dual-linear polarization (DLP), circular polarization (CP), dual-circular polarization (DCP), and pattern reconfigurability [27]-[30]. Considering the above ideas, a single HDA with DCP property is very promising. To the best of our knowledge, only one antenna reported in the current literature [30] has achieved DCP performance with an electrically small size. It combines two space-separated Huygens CP (HCP) antennas with 45° rotation offset that are excited individually by two feed networks. The radiators consist of six substrate layers while the shared-radiator in this work only has three layers with a totally different operating mechanism. Moreover, the peak realized gain values (less than 2 dBic) of the design in [30] are lower than this work due to the use of much more pieces of substrates that features a high design complexity and cost.

In this Communication, a novel electrically small Huygens DCP (HDCP) antenna operating at 915 MHz ISM (industrial, scientific, and medical) band is developed that features an ultracompact size, i.e., π (0.12 λ_c)² × 0.06 λ_c = 0.0027 λ_c ³ (ka = 0.78). An antenna is defined as electrically small if ka < 1, where k is the wavenumber and a is the smallest sphere that encloses the entire antenna. HDCP radiation characteristics are achieved for the first time using a single shared-radiator. This approach eliminates the need for two separated HCP antennas, as used in [30]. A simulated (measured) maximum realized gain of 3.39 dBic (2.8 dBic) and a good port isolation of higher than 16 dB is achieved. It is realized by two pairs of orthogonally oriented capacitively loaded loops (CLLs) and Egyptian axe dipoles (EADs), forming a shared-radiator for DCP beams. An '8' shaped feeding structure as the driven element is adopted. To compensate for the inductive impedance at the two ports, an innovative compact LC matching network is designed that successfully transforms the impedance to standard 50 Ω . The rest of the Communication is structured as follows. Sec. II describes the antenna configuration. Sec. III demonstrates the design evolution process and performance. The fabrication, simulated, and measured results are discussed in Sec. IV. Finally, conclusions are summarized in Sec. V.

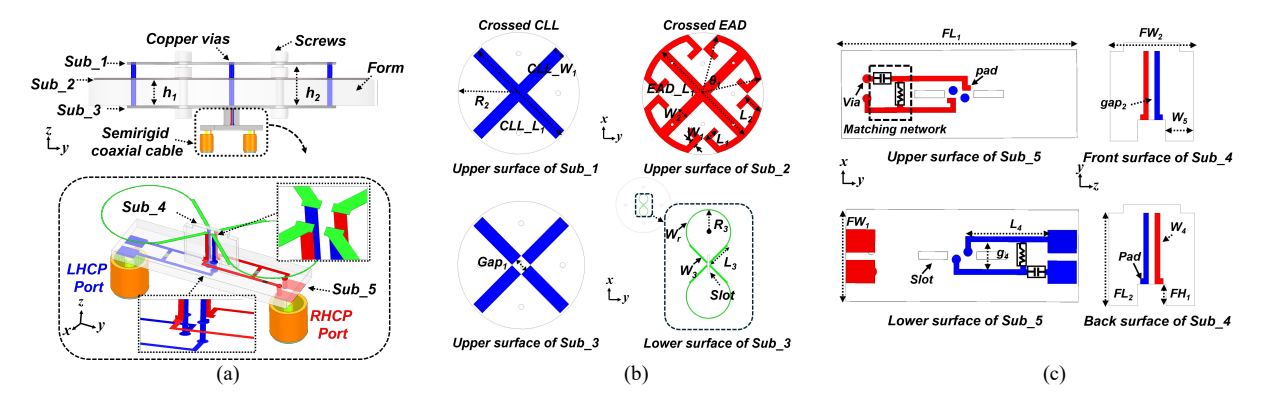


Fig. 1 Configuration of the proposed electrically small shared-radiator HDCP antenna. (a) Side view and detailed view. (b) Detailed configuration of the radiating element. (c) Detailed configuration of the compact LC matching network.

II. CONFIGURATION OF THE SHARED-RADIATOR ELECTRICALLY SMALL HUYGENS DUAL-CP (HDCP) ANTENNA

Fig. 1 illustrates the detailed geometry of the electrically small shared-radiator HDCP antenna. As shown in Fig. 1 (a), the antenna system consists of five pieces of dielectric substrate, and they are labeled as Sub_1 to Sub_5. Specifically, it can be divided into two parts: the radiating part (Sub 1 to Sub 3) and the LC matching network part (Sub 4 to Sub 5). The shared-radiator mainly consists of two pairs of orthogonally oriented capacitively loaded loops (CLLs) and Egyptian axe dipoles (EADs). They are systematically integrated into the radiating entity by three substrates. As shown in Fig. 1 (b), the copper strips of the crossed CLLs are etched on the upper surface of both Sub 1 and Sub 3. Then, four vertical connecting copper rods, each with a 1.5mm diameter, connect the strips through the Sub 1 and Sub 2 to form two complete CLLs. The copper strips of the crossed EADs are etched onto the upper surface of Sub_2. To prevent short-circuit with the crossed CLLs, four circular holes around the copper rods, each with a 2 mm diameter, were removed from the crossed EADs.

The compact LC matching feed network consists of two differential input ports as shown in Fig. 1 (a). For convenient processing, the '8'-shaped feed line as the driven element is etched at the lower surface of Sub 3. It includes two orthogonally-arranged short dipoles that utilize two small loops to form a short terminal. Two pairs of vertical differential transition lines (shown in red and blue) are etched on both sides of Sub 4 to connect the two ports of the short dipoles on Sub_3. Subsequently, two pairs of horizontal differential lines etched on top and bottom surfaces of another substrate (Sub 5) are designed to connect the vertical transition lines. They incorporate two pairs of LC matching networks (L = 70 nH, C= 0.9 pF) on each surface of Sub_5, along with four copper vias connecting to the two pairs of vertical differential transition lines. Moreover, three rectangular slots (one of the slots is excavated in Sub 3 and the other two are in Sub 5) and several forms are used to enable the mechanical stability of the feed network in the fabrication and measurement processes. Detailed configuration is illustrated in Fig. 1 (c). All these substrates are F4B with a relative dielectric constant of 2.2, a loss tangent of 0.003, and a cladding copper thickness of 0.017mm. Sub_1 and Sub_3, Sub_2 and Sub 4 have the same thickness, which are 0.8 mm and 0.5 mm, respectively. The thickness of Sub 5 is 1.5mm. Besides, a cylindrical grid form is used to support Sub 2 and ensure the accurate relative vertical distance between Sub 1 and Sub 3. Four screws are placed at four certain

corners and go through Sub_1 to Sub_3 to ensure the stability of the assembled antenna system.

The detailed analysis and operating mechanisms of the CLLs and EADs elements together with their design guidelines to construct a Huygens dipole antenna (HDA) have been thoroughly discussed in [26], thus they are not reiterated here to avoid redundancy. All the corresponding design parameters have been optimized by Ansys HFSS and are listed as follows: h_1 = 7.64 mm, h_2 = 12.04 mm, R_2 = 30.7 mm, CLL_W_1 = 6 mm, CLL_L_1 = 59.1 mm, EAD_L_1 = 80.5 mm, W_1 = 4 mm, W_2 = 7mm, L_1 = 10.4 mm, L_2 = 13.4 mm, θ_1 = 31, Gap_1 = 6.5 mm, W_r = 0.15 mm, W_3 = 0.36 mm, L_3 = 5.5 mm, R_3 = 5 mm, FL_1 = 16 mm, FL_2 = 7.124 mm, FW_1 = 6 mm, FW_2 = 6 mm, W_4 = 0.36 mm, L_4 = 6.5 mm, g_4 = 1.8 mm, FH_1 = 1.524 mm.

III. OPERATING PRINCIPLE AND KEY DESIGN CONSIDERATIONS OF THE SHARED-RADIATOR ELECTRICALLY SMALL HDCP ANTENNA

In this section, the operating mechanism and key design considerations of the HDCP antenna are investigated. To achieve DCP beams, a symmetric '8'-shaped feed line with two orthogonal ports was introduced to excite the crossed-shaped Huygens shared-radiator. High isolation between two CP ports is realized naturally. Due to the extended delay line in the feed structure, the impedances show high inductance. To compensate for the inductive impedance, two pairs of differential lines (blue and red lines as shown in Fig. 1 (a)) perpendicular to the '8'-shaped feed line are employed to connect the two orthogonal ports and extend horizontally to form two solderable independent ports. Finally, two LC matching networks (inside the black dotted box as shown in Fig. 1 (c)) are incorporated to ensure a good impedance matching with the standard 50 Ω transmission line.

A. Operating principle of the shared-radiator excited by an '8'-shaped feed line for realizing DCP Huygens beams

Fig. 2 shows the symmetric '8'-shaped feed line with two orthogonal ports. Simultaneously, the 90° phase difference required for CP radiation is provided by the curves (delayed loop) that connect the two pairs of orthogonal short dipoles in series. For convenience, two lumped ports are used as the differential sources in this section to investigate the variation of current distributions on all components and port isolation. It should be noted that Port#1 is assigned to the top surface of the copper strip, while Port#2 is assigned 0.017 mm lower on the bottom surface of the copper strip (i.e., the thickness of the copper strip is 0.017 mm).

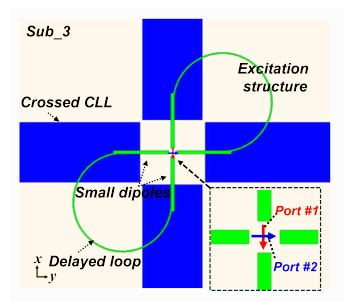


Fig. 2. Configuration of the '8'-shaped feed line as the driven element designed on the lower surface of Sub~3.

When one port of the '8'-shaped feed line is driven while the other is matched, orthogonal loop currents with 90° phase difference on the crossed CLL elements are excited, which function as two orthogonal magnetic dipoles. The crossed EADs are mainly excited through their coupling with the currents on the upper sections of the crossed CLLs, acting as two orthogonal electrical dipoles. When the two pairs of orthogonally oriented CLLs and EADs are properly excited with a 90° phase difference by the two ports of the '8'-shaped feed line, the DCP radiation can be achieved. To clarify the operational mechanisms of the two polarization states, the current distributions on the shared-radiator and the feed line were simulated for each state. The surface current distributions on the feed line, CLLs, and EADs at four moments in a period of time T, i.e., 0, T/4, T/2, and 3T/4, are highlighted in Fig. 3. As an example, the red arrows on the CLLs and EADs indicate that their current vector direction along the y- and xaxis rotates in the clockwise direction, as shown in Fig. 3(a). Thus, the RHCP radiation is generated and has its maximum beam pointing at the +z-direction. Similarly, the current vector along the x- and yaxis rotates in the counterclockwise direction to create LHCP radiation. As shown in

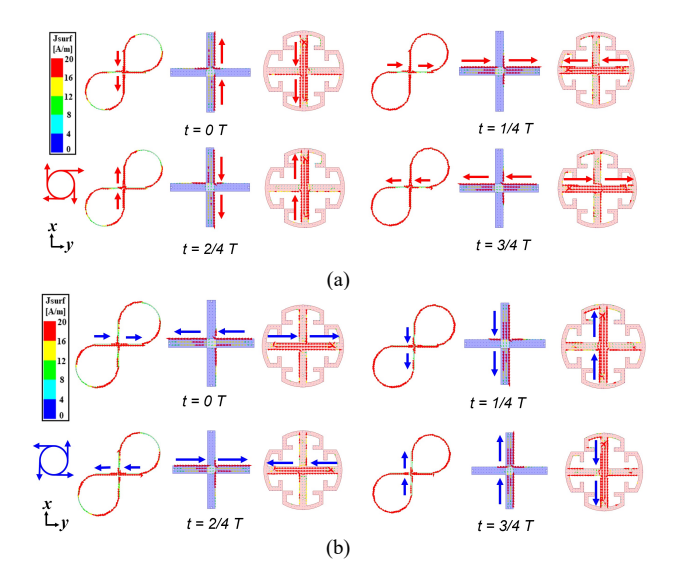


Fig. 3. Simulated surface current distributions on the driven element, Top strip of the CLL, and EAD for the electrically small HDCP antenna. (a) RHCP when *port #1* is excited and *port #2* is matched. (b) LHCP when *port #2* is excited and *port #1* is matched.

Fig. 4 (a), axial ratio (AR) values less than 3 dB around 915 MHz for both CP states are achieved. Although the two ports might appear to be physically short-circuited by the driven feed line, the achieved isolation is very good and is facilitated by the orthogonal nature of the two CP states. To be more specific, as shown in Fig. 3, the

current vectors on the CLLs in both CPs are always orthogonal at the same moment due to the orthogonal feeding approach. For instance, at t = 0 T, the current vectors (red arrows) on the CLLs are oriented along the x-axis for RHCP radiation, whereas the current vectors (blue arrows) on the CLLs are oriented along the y-axis for LHCP radiation, and hence the good isolation between the two ports is achieved. The simulated isolation between both ports when port#1 is excited and port#2 is matched is presented in Fig. 4 (b) to prove the statement. It shows that the best port isolation value is larger than 40 dB at 918 MHz. At our targeted 915 MHz, the port isolation is also good, e.g., larger than 20 dB, which satisfies the requirements for DCP radiation. Due to the symmetric feeding structure, only the simulated RHCP Huygens radiation pattern and AR beamwidth at two vertical planes are given in Fig. 5. Its radiation patterns are almost identical at two vertical planes with a peak gain value being 3.71 dBic and a wide 132° HPBW (3 dB), from \pm 66°. Fig 5 (d) shows the wide Axial ratio beamwidth, which is wider than the HPBW. So, a wide overlapped beamwidth of 132° is achieved.

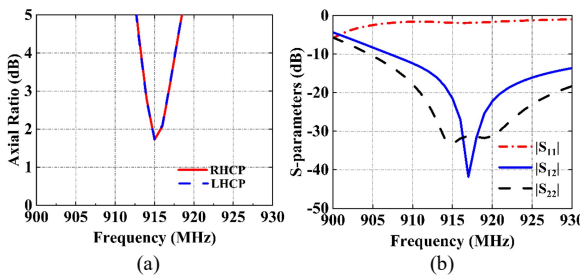


Fig. 4. Simulated axial ratio and isolation as functions of source frequency for the electrically small HDCP antenna. (a) Axial ratio at $\varphi = 0^{\circ}$, $\theta = 0^{\circ}$ for both CPs. (b) Port isolation when *port #1* is excited and *port #2* is matched.

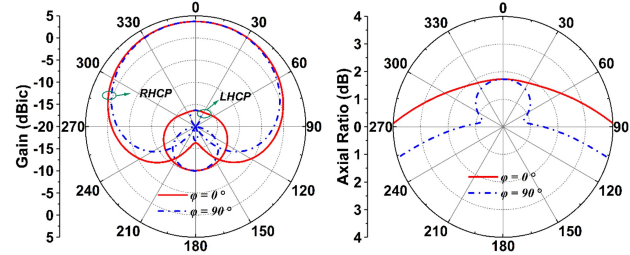


Fig. 5. Simulated radiation pattern at two vertical planes at 915 MHz when port #1 is excited and port #2 is matched. (a) Gain. (b) Axial ratio beamwidth.

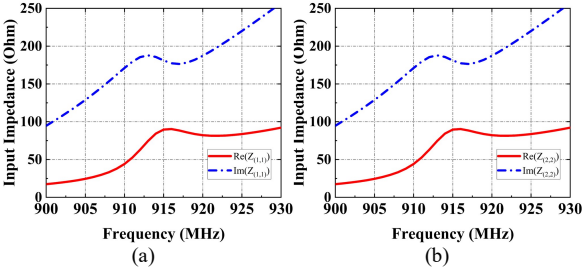


Fig. 6. Simulated input impedance as functions of the source frequency for the electrically small HDCP antenna. (a) Port #1 is excited and *port* #2 is matched. (b) Port #2 is excited and *port* #1 is matched.

B. Key design considerations of the LC matching network

The simulated results show that good DCP performance is realized by exciting each lumped port of the '8'-shaped feed line. The corresponding simulated input impedances as functions of source frequency for both ports are also given in Fig. 6. It is observed that the impedance for both ports is $93 + j180~\Omega$ at 915 MHz. Note that the impedance exhibits high input inductance, which

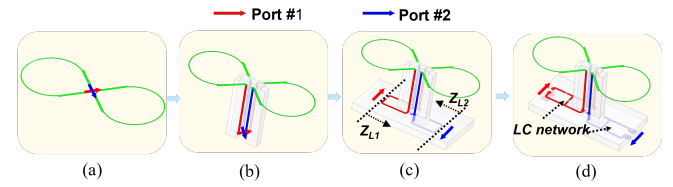


Fig. 7. Evolution of the proposed compact feeding structure. (a) '8'-shaped feed-line structure with two orthogonal ports. (b) A vertical board with two pairs of vertical differential lines. (c) A horizontal board with two pairs of differential lines. (d) with LC components for the antenna impedance matching.

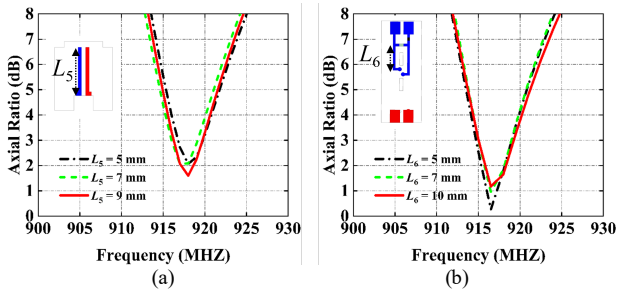


Fig. 8. Simulated axial ratio as functions of the source frequency. (a) axial ratio values for different length of L_5 . (b) axial ratio values for different length of L_6 .

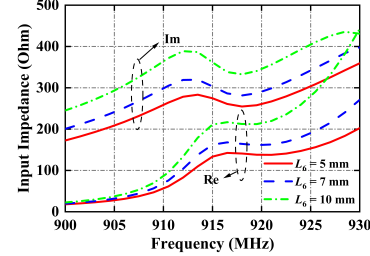


Fig. 9. Simulated input impedance as functions of the source frequency for different length of L_6 .

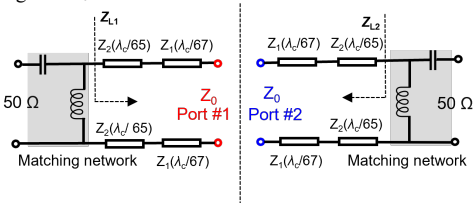


Fig. 10. Schematic of the proposed compact feeding network.

arises from the '8'-shaped feed line, generating strong parasitic inductances. Additionally, it should be noted that the lumped ports are ideal sources in the full-wave simulator. In practice, however, it is very difficult to excite the ports as they interfere with each other (e.g., overlap on the same location) as shown in Fig. 7 (a). Thus, conventional excitation methods in [31], [32] are not feasible due to the limited physical size (e.g., The length of a short dipole is only $0.036~\lambda c$). To address these issues, an innovative compact feed network was designed.

Fig. 7 shows the design evolution process of the entire feeding structure. Firstly, four vertically orientated differential lines beneath the '8'-shaped feed line were designed. They act as a transition between the excitations for the share-radiator and the LC matching network. To ensure the feasibility of the feed network, the length variation of the differential lines on its AR values in the broadside direction is also discussed. As shown in Fig. 8, the length variations of L_5 and L_6 have less impact on the CP performance. This is because the amplitude and phase of the excitations (differential lines) at the

ports of the '8'-shaped feed structure are still balanced. Moreover, for clarity, only the impedance variation with L_6 is shown in Fig. 9. It can be observed that the length variation will affect the input impedance of the antenna and the impedance also exhibits high inductance at 915 MHz. So, the impedances (Z_{L1} and Z_{L2}) at the ports shown in Fig. 7 (c) require LC matching networks. In fact, they (Z_{L1} and Z_{L2}) can be easily got in a full wave simulator once the length of L5 and L6, as shown in Fig. 8, is determined. Then, based on the calculation in the Smith chart, L = 70 nH, C = 0.9 pF in the LC matching network was chosen to transform the impedance to 50 Ω . In this regard, Fig. 10 presents the schematic of the dual ports feeding network, which clearly shows the impedance matching process of the proposed feeding structure.

Finally, a compact feed network was successfully realized in this work. The issue of overlapping ports at the '8'-shaped feed structure was solved, and a port resistance of 50 Ω at 915 MHz was also achieved through the compact LC matching network. When different ports are excited, the broadside LHCP or RHCP radiation and good impedance matching can be easily obtained.

IV. FABRICATION AND MEASUREMENT RESULTS OF THE SHARED-RADIATOR ELECTRICALLY SMALL HDCP ANTENNA

To validate the performance of the electrically small HDCP antenna, its prototype was fabricated and measured. The photograph of the assembled prototype is given in Fig. 11 along with the test environment in an anechoic chamber. Two semirigid 50 Ω coaxial cables with classical quarter-wavelength sleeve baluns operated as RF choke are employed to feed the antenna. Moreover, for facilitating antenna assembly and maintaining the relative vertical distance between the different layers, four screws and a cylindrical form are used to assemble the separated layers.

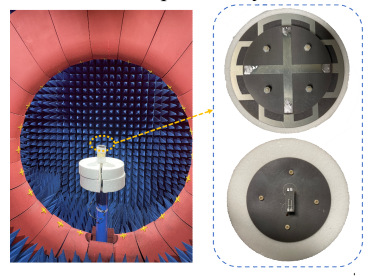


Fig. 11. Photo of the proposed ultracompact shared-radiator HDCP antenna.

The simulated and measured S-parameters and realized gain values of the electrically small HDCP antenna at two ports as functions of the source frequency are plotted in Fig. 12. As seen, the simulated and measured return loss of the two ports differed somewhat from each other, but the trend of the measured results aligns well with the simulated results. The measured fractional impedance bandwidths ($|S_{nn}| < -10 \text{ dB}$, n = 1, 2) for LHCP (Port 2) and RHCP (port 1) are the same, 3.2%. Moreover, the simulated isolation between the two ports has a minimum value of 19 dB at 915 MHz, for the measured results the optimum isolation is 16 dB and shifted to 917 MHz, but it is still better than the standard requirement of 15dB for DCP antennas. The simulated (measured) 15 dB isolation bandwidth between two ports is approximately 0.44% (0.54%) from 914 (915 MHz) to 918 MHz (920 MHz). Moreover, Fig. 9 also shows that the simulated (measured) peak realized gain for LHCP and RHCP are 3.39 (2.82) and 3.32 (2.63) dBic, respectively, with both states exhibiting a total efficiency of approximately 70%.

 $\pi (0.12 \lambda_c)^2 \times 0.06 \lambda_c =$

0.0027 λ

Ref.

[9]

[11]

[12]

This

Work

0.

0.5

0.4

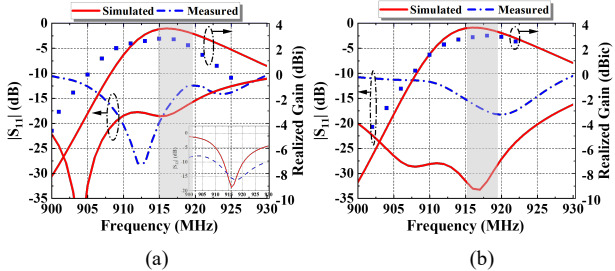
PERFORMANCE COMPARISON OF THE PROPOSED ELECTRICALLY SMALL DCP ANTENNAS BROADSIDE BEAMS						
Antenna Volume (λ_c^3)	Antenna type	ka	Peak RG (dBic)	Overlapped Bandwidth (%)	Isolation (dB)	Shared-Radiator
$0.5 \lambda_c \times 0.5 \lambda_c \times 0.057 \lambda_c$ $= 0.014 \lambda_c^3$	Ring-slot loaded with AMC	2.16	6	4	>16	Yes
$53 \lambda_c \times 0.53 \lambda_c \times 0.035 \lambda_c$ $= 0.01 \lambda_c^3$	SIW backed cavity	2.45	5.22	8.4	>24	Yes
$41 \lambda_c \times 0.41 \lambda_c \times 0.025 \lambda_c$ $= 0.004 \lambda_c^3$	Microstrip patch	1.82	3	NG	>30	Yes
$\pi (0.15 \lambda_c)^2 \times 0.053 \lambda_c = 0.0037 \lambda_c^3$	Huygens dipole antenna	0.94	1.81	0.99	>15.6	No

2.82 (Meas.)

3.39 (Sim.)

TABLE I PERFORMANCE COMPARISON OF THE PROPOSED ELECTRICALLY SMALL DCP ANTENNAS BROADSIDE BEAMS

0.78



Huygens dipole

antenna

Fig. 12. Simulated and measured reflection coefficients and realized gains as functions of the source frequency for the proposed electrically small shared-radiator HDCP antenna. (a) LHCP. (b) RHCP.

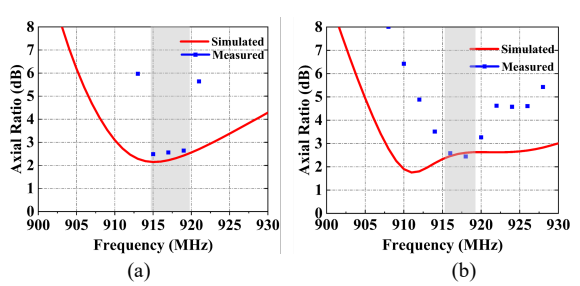


Fig. 13. Simulated and measured axial ratio values as functions of the source frequency. (a) AR values for LHCP radiation. (b) AR values for RHCP radiation.

It is observed that the measured realized gain is slightly lower than the simulated one, which would be due to the imperfect manual welding during the assembly process and the distorted impedance matching (compared with the simulated one). Fig. 13 shows that the measured overlapped AR bandwidth for the two polarizations is about 0.44% from 915 to 919 MHz. The discrepancies between the measured and simulated results may be attributed to the fabrication and measurement tolerances. In addition, with $|S_{nn}| < -10$ dB (n = 1, 2), AR < 3 dB, and isolation > 15 dB, the measured overlapped bandwidth for both polarizations is 0.44% (915-919 MHz). Moreover, the antenna is electrically small with $ka \sim 0.78$ (915 MHz).

Fig. 14 shows the simulated and measured normalized radiation patterns at two vertical planes ($\varphi=0^\circ$ and $\varphi=90^\circ$) of the electrically small HDCP antenna. It can be predicted that the proposed antenna features symmetrical radiation patterns and lower cross-polarization than -15 dB at the maximum radiation direction. When port 1 was excited, the broadside RHCP radiation characteristic is obtained, and we can find the measured results are well matched with the simulated ones. Besides, the simulated (measured) 3 dB AR beamwidth is about 194° (150°) from -99° (-90°) to 95° (60°) at $\varphi=0^\circ$ and 144° (120°) from -69° (-60°) to 75° (60°) at $\varphi=90^\circ$.

Similarly, when port 2 was excited, the broadside LHCP radiation characteristic was obtained. However, apart from the back-lobe, the simulated cross-polarization results are reasonably consistent with the measured ones. And the simulated (measured) 3 dB AR beamwidth is about 121° (75°) from -70° (-30°) to 51° (45°) at $\varphi = 0^\circ$ and 190° (120°) from -87° (-60°) to 93° (60°) at $\varphi = 90^\circ$.

>16

Yes

0.44 (Meas.)

1.3 (Sim.)

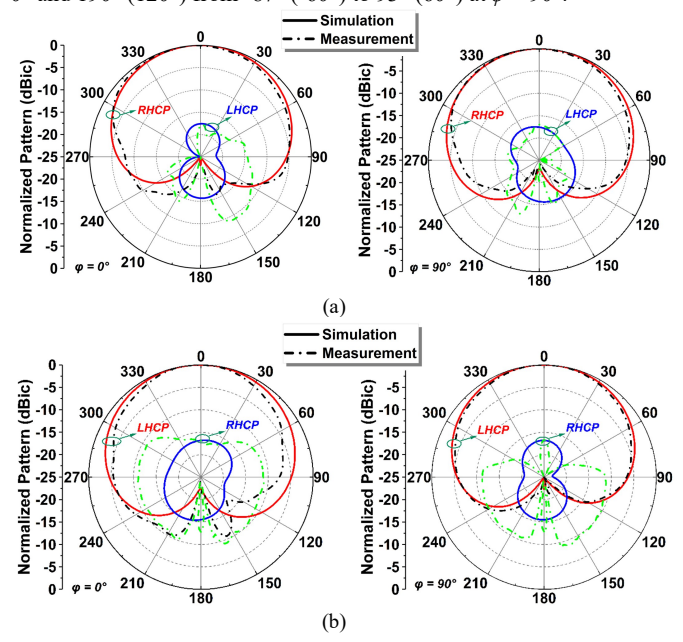


Fig. 14. Simulated and measured realized gain patterns of the proposed electrically small HDCP antenna. (a) RHCP. (b) LHCP.

Table I is a comparison of the antenna type and major performances between the proposed DCP antenna with other reported designs in the open literature. Importantly, the DCP antenna demonstrated in this work is the first-of-its-kind antenna to realize the DCP characteristics based on one single Huygens shared-radiator antenna. In comparison, the proposed antenna has demonstrated the advantages including the smallest volume (0.0027 λ_c^3), electrically small size (ka = 0.78), and good isolation between two ports. The design in [30] achieves the DCP characteristics with an electrically small size, ka = 0.91, but the structure features a high design complexity and cost, as well as lower gain. In particular, its radiators consist of six substrate layers while the shared-radiator only has three substrate layers. This also causes its peak realized gain to be just 1.81 dBic, considerably less than the 2.82 dBic achieved by our shared-radiator design. Overall, instead of separately exciting two space-separated Huygens CP (HCP) antennas with 45° rotation offset, our developed Huygens shared-radiator antenna achieves DCP performance more efficiently with a compact feeding network.

It should be noted that electrically small antennas typically have narrow bandwidths, as demonstrated in the previous works [26] - [30]. For practical applications, we intend to use the developed antenna for wireless power transfer applications in battery-free IoT ecosystems, in which the current bandwidth is sufficient.

V. CONCLUSION

In this Communication, an ultracompact electrically small DCP antenna based on one single Huygens shared-radiator is presented for the first time. The method of using an '8'-shaped feed-line as the driven element to excite DCP radiation, along with an innovative and compact LC matching network to compensate for the inductive impedance of the two ports, was explained. The working mechanism and key design considerations of the antenna have been carefully studied to establish engineering design guidelines. Measured results show a reasonable agreement with the simulated ones. In summary, the proposed HDCP antenna features an ultracompact structure, electrically small size, and wide beamwidth. These merits position the proposed antenna as a good candidate for various narrowband wireless systems that require a compact footprint and large DCP signal coverage. e.g., Compact IoT system that integrates sensing and communication.

REFERENCES

- [1] Z. Wang, S. Liu, and Yuandan Dong, "Electrically small, low-Q, widebeam-width, circularly polarized, hybrid magnetic dipole antenna for RFID application," *IEEE Trans. Antennas Propag.*, vol. 69, no. 10, pp. 6284–6293, Oct. 2021.
- [2] W. Lin, R. W. Ziolkowski, and M. -C. Tang, "Circularly polarized electrically small antennas for emerging wireless applications," 12th European Conference on Antennas and Propagation (EuCAP 2018), London, UK, 2018, pp. 1-4.
- [3] W. Lin, R. W. Ziolkowski and J. Huang, "Electrically small, low-Profile, highly efficient, Huygens dipole rectennas for wirelessly powering Internet-of-Things devices," *IEEE Trans. Antennas Propag.*, vol. 67, no. 6, pp. 3670-3679, June 2019.
- [4] S. Gao, Q. Luo, and F. Zhu, Circularly Polarized Antennas, Hoboken, NJ, USA:Wiley, 2013.
- [5] H. Li, B. Wang, Z. Hu, and W. Lin, "A four-arm electrically small omnidirectional CP helical antenna and Its expansion as a compact and highly efficient dual-CP array," *IEEE Trans. Antennas Propag.*, vol. 71, no. 9, pp. 7081-7090, Sept. 2023.
- [6] S. Liu, Z. Wang and Y. Dong, "Electrically small circularly polarized antenna based on capacitively loaded loop," *IEEE Antennas and Wireless Propag. Letters*, vol. 21, no. 9, pp. 1767-1771, Sept. 2022.
- [7] S. Gao, A. Sambell, and S. S. Zhong, "Polarization-agile antennas," IEEE Antennas Propag. Mag., vol. 48, no. 3, pp. 28–37, Jun. 2006.
- [8] W. Zeng, X. Wu, F. Wu, Y. Zhang, Z. Jiang, and W. Hong, "Broadband dual-CP multistage sequential rotation arrays with independent control of polarizations based on dual-CP magnetoelectric dipole elements," *IEEE Trans. Antennas Propag*, vol. 72, no. 4, pp. 3017-3032, April 2024.
- [9] R. Ferreira, J. Joubert, and J. W. Odendaal, "A compact dual-circularly polarized cavity-backed ring-slot antenna," *IEEE Trans. Antennas Propag.*, vol. 65, no. 1, pp. 364-368, Jan. 2017
- [10] H. H. Tran, N. Nguyen-Trong, and H. C. Park, "A compact dual Circularly polarized antenna with wideband operation and high isolation," *IEEE Access*, vol. 8, pp. 182959-182965, 2020.
- [11] Y. -D. Yan, Y. -C. Jiao, H. -T. Cheng, and C. Zhang, "A low-profile dual-circularly polarized wide-axial-ratio-beamwidth slot patch antenna with six-port feeding network," *IEEE Antennas and Wireless Propag. Letters*, vol. 20, no. 12, pp. 2486-2490, Dec. 2021.
- [12] Y. He, C. Gu, H. Ma, J. Zhu, and G. V. Eleftheriades, "Miniaturized circularly polarized Doppler radar for human vital sign detection," *IEEE Trans. Antennas Propag.*, vol. 67, no. 11, pp. 7022-7030, Nov. 2019.
- [13] J. Wu, W. Yang, L. Gi, Q. Xue, and W. Che, "Low-profile wideband dual-circularly polarized metasurface antenna based on traveling-wave sequential feeding mechanism," *IEEE Antennas and Wireless Propag. Letters*, vol. 21, no. 6, pp. 1085-1089, June 2022.

- [14] Y. -H. Yang, J. -L. Guo, B. -H. Sun, Y. -M. Cai, and G. -N. Zhou, "The design of dual circularly polarized series-fed arrays," *IEEE Trans. Antennas Propag.*, vol. 67, no. 1, pp. 574-579, Jan. 2019.
- [15] C. Zhang, X. Liang, X. Bai, J. Geng, and R. Jin, "A broadband dual circularly polarized patch antenna with wide beamwidth," *IEEE Antennas and Wireless Propag. Letters*, vol. 13, pp. 1457-1460, 2014.
- [16] S. J. Chen, C. Fumeaux, Y. Monnai, and W. Withayachumnankul, "Dual circularly polarized series-fed microstrip patch array with coplanar proximity coupling," *IEEE Antennas and Wireless Propag. Letters*, vol. 16, pp. 1500-1503, 2017.
- [17] D. Wu, J. Liang, and L. Ge, "A wideband dual-circularly polarized series-fed corner-truncated patch array using coplanar proximity coupling," *IEEE Trans. Antennas Propag.*, vol. 72, no. 4, pp. 3292-3301, April 2024.
- [18] Y. Cheng, and Y. Dong, "Dual circularly polarized broadband antenna array for millimeter-wave applications," *IEEE Antennas and Wireless Propag. Letters*, vol. 21, no. 12, pp. 2377-2381, Dec. 2022.
- [19] L. Lu, Y. -C. Jiao, W. Liang, and H. Zhang, "A novel low-profile dual circularly polarized dielectric resonator antenna," *IEEE Trans. Antennas Propag.*, vol. 64, no. 9, pp. 4078-4083, Sept. 2016.
- [20] H. D. Li, X. Y. Du, J. Y. Yin, J. Ren, and Y. Yin, "Differentially fed dual-circularly polarized antenna with slow wave delay lines," *IEEE Trans. Antennas Propag.*, vol. 68, no. 5, pp. 4066-4071, May 2020.
- [21] C. Mao, M. Khalily, R. Tafazolli and A. Kishk, "Wideband dual circularly polarized helical antenna with reduced mutual coupling for MIMO applications," *IEEE Trans. Antennas Propag.*, vol. 72, no. 4, pp. 3766-3771, April 2024.
- [22] C. Mao, M. Khalily, R. Tafazolli, and A. Kishk, "Wideband dual circularly polarized helical antenna array for satellite applications," *IEEE Antennas and Wireless Propag. Letters*, vol. 23, no. 9, pp. 2758-2762, Sept. 2024.
- [23] M. Almalki, and S. K. Podilchak, "Wideband multiport antenna design by sub-array aperture sharing offering dual-circularly polarized beamforming for wireless power transfer," *IEEE Antennas and Wireless Propag. Letters*, doi: 10.1109/LAWP.2024.3408450.
- [24] H. D. Le, T. Le-Huu, K. K. Nguyen, and S. X. Ta, "Dual circularly polarized fabry–perot antenna using single-layer self-polarizing PRS," *IEEE Antennas and Wireless Propag. Letters*, vol. 22, no. 10, pp. 2575– 2579. Oct. 2023.
- [25] C. Shu, S. Hu, X. Cheng, A. S. Andy, Y. Yao, B. Zhang, Y. Alfadhl, and X. Chen, "Wideband dual-circular-polarization antenna with high isolation for millimeter-wave wireless communications," *IEEE Trans. Antennas Propag.*, vol. 70, no. 3, pp. 1750-1763, March 2022.
- [26] R. W. Ziolkowski, "Low Profile, Broadside Radiating, Electrically Small Huygens Source Antennas," in IEEE Access, vol. 3, pp. 2644-2651, 2015.
- [27] M. -C. Tang, Z. Wu, T. Shi, H. Zeng, W. Lin, and R. W. Ziolkowski, "Dual-linearly polarized, electrically small, low-profile, broadside radiating, Huygens dipole antenna," *IEEE Trans. Antennas Propag.*, vol. 66, no. 8, pp. 3877-3885, Aug. 2018.
- [28] W. Lin, and R. W. Ziolkowski, "Electrically small, low-profile, Huygens circularly polarized antenna," *IEEE Trans. Antennas Propag.*, vol. 66, no. 2, pp. 636–643, Feb. 2018.
- [29] W. Lin, and H. Li, "Ultracompact pattern-reconfigurable Huygens dipole antenna with uniform polarization and quasi-isotropic coverage," *IEEE Trans. Antennas Propag.*, vol. 72, no. 6, pp. 4940-4950, June 2024.
- [30] Z. Wu, M. -C. Tang, T. Shi, and R. W. Ziolkowski, "Two-port, dual-circularly polarized, low-profile broadside-radiating electrically small Huygens dipole antenna," *IEEE Trans. Antennas Propag.*, vol. 69, no. 1, pp. 514-519, Jan. 2021.
- [31] W. Lin, and R. W. Ziolkowski, "Compact, high directivity, omnidirectional circularly polarized antenna array," *IEEE Trans. Antennas Propag.*, vol. 67, no. 7, pp. 4537-4547, July 2019.
- [32] R. Li, T. Wu, B. Pan, K. Lim, J. Laskar, and M. M. Tentzeris, "Equivalent-circuit analysis of a broadband printed dipole with adjusted integrated balun and an array for base station applications," *IEEE Trans. Antennas Propag.*, vol. 57, no. 7, pp. 2180-2184, July 2009.